

---

# polyGen - A Learning Framework for Atomic-level Polymer Structure Generation

---

**Ayush Jain**

School of Materials Science and Engineering  
Computational Science and Engineering  
Georgia Institute of Technology  
ayush.jain@gatech.edu

**Rampi Ramprasad**

School of Materials Science and Engineering  
Georgia Institute of Technology  
rampi.ramprasad@mse.gatech.edu

## Abstract

Synthetic polymeric materials underpin fundamental technologies in the energy, electronics, consumer goods, and medical sectors, yet their development still suffers from prolonged design timelines. Although polymer informatics tools have supported speedup, polymer simulation protocols continue to face significant challenges: on-demand generation of realistic 3D atomic structures that respect the conformational diversity of polymer structures. Generative algorithms for 3D structures of inorganic crystals, bio-polymers, and small molecules exist, but have not addressed synthetic polymers. In this work, we introduce polyGen, the first latent diffusion model designed specifically to generate realistic polymer structures from minimal inputs such as the repeat unit chemistry alone, leveraging a molecular encoding that captures polymer connectivity throughout the architecture. Due to a scarce dataset of only 3855 DFT optimized polymer structures, we augment our training with DFT-optimized molecular structures, showing improvement in joint learning between similar chemical structures. We also establish structure matching criteria to benchmark our approach on this novel problem. polyGen effectively generates diverse conformations of both linear chains and complex branched structures, though its performance decreases when handling repeat units with a high atom count. Given these initial results, polyGen represents a paradigm shift in atomic level structure generation for polymer science—the first proof-of-concept for predicting realistic atomic-level polymer conformations while accounting for their intrinsic structural flexibility.

## 1 Introduction

Polymeric materials play a central role in modern science and engineering, enabling technologies across sectors such as packaging, electronics, medicine, and energy. [1, 2] Their versatility arises from the vast structural diversity of organic building blocks [3], the ingenuity of synthetic chemistry, and the breadth of accessible processing techniques. By tuning parameters such as monomer composition, chain architecture, additives, and processing conditions, polymers can be engineered to span a wide range of mechanical, electrical, and transport properties—from rigid plastics, elastomers, dielectrics [4], and membranes [5, 6, 7]. Despite the impact of polymers, the discovery and deployment of new materials remains a slow and resource-intensive process. This is due to the vastness of chemical and processing design spaces [8] and the need to balance performance, cost, safety, and manufacturability. As a result, polymer innovation still relies heavily on experience, trial-and-error, chemical intuition, and serendipity. Novel methods of generating polymer designs guided by informatics approaches have emerged, such as virtual forward synthesis, evolutionary algorithms, and syntax-directed autoencoders that can produce a theoretically innumerable amount of polymer candidates [9, 1, 10, 11]. Physics-based computer simulations may accelerate the pace of polymer discovery but these methods also

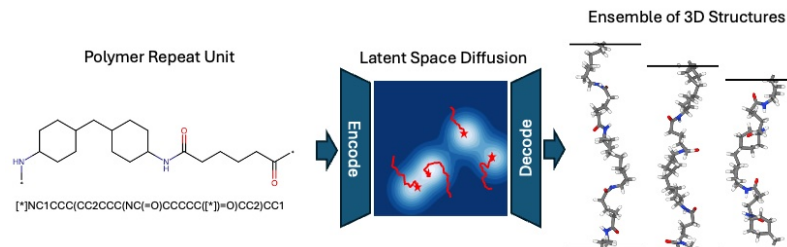


Figure 1: Theoretical overview of polyGen from the perspective of chemistry-conditioned energy minimization of the potential energy surface represented in the latent space. With this capability, an initial connectivity for a polymer repeat unit can be used to generate structures with a high probability of being at a potential energy minimum.

face barriers that have thus far prevented the widespread utilization of such approaches as detailed below.

A key challenge faced by the polymer simulation community is the creation of suitable initial atomic-level structures especially for novel chemistries. Unlike crystalline inorganic materials, polymers exhibit a complex combination of amorphous, semicrystalline, and crystalline domains, with conformational flexibility and structural disorder playing essential roles in their function [12]. Currently, Polymer Structure Predictor (PSP) [13] is a physics and heuristic-based framework that can generate initial structures of polymers to be used as inputs to Density Functional Theory (DFT) or Molecular Dynamics (MD) simulations. However, rapidly producing statistically diverse and realistic conformations requires accounting for the many low-energy conformations that a polymer can adopt. As illustrated in Figure 1, there is a growing need for predictive tools that can generate realistic 3D atomic structures of polymers from minimal inputs, such as chemical composition or connectivity (e.g., SMILES). Such tools would enable property prediction, surrogate simulation, and rational design faster in the discovery pipeline.

**Generative Materials Structure Prediction** Materials generation via diffusion models [14] or flow matching [15] offers promise. Typically, these models use datasets containing structures optimized by DFT [16] or MD simulations [17]. With materials research, these methods have been used thus far for inorganic crystalline materials with a finite number of atoms within a unit cell parameterized by the lattice angles and lengths [18, 19, 20]. Significant progress has also emerged in structure prediction for large biological polymers, particularly proteins, where models like AlphaFold [17, 21] and Boltz-1 [22] can now generate accurate three-dimensional conformations from amino acid sequences. Similarly, the generation of small molecule conformers [23, 24, 25] has also been an open problem, especially in the context of protein docking [26].

The synthetic polymers generation problem is a mix of all of these applications. Similar to crystals, synthetic polymers can be defined by a periodic unit. 3D structures of these repeat units are also defined within unit cells/bounding boxes [12]. Traditional crystal structure prediction methods, while powerful for smaller systems, have not displayed abilities to capture the rich conformational landscape of polymers. The local features of synthetic polymers are more akin to molecules where the local (short-range) connectivity of their structures is well-defined. However, polymers occur as long chains composed of sequences of 10s-10,000s of monomeric repeat units, which necessitates an understanding of longer-range interactions for stochastic structure generation. This is similar to protein modeling approaches like AlphaFold3, which employs diffusion transformers to predict an ensemble of structures [21]. However, unlike proteins, which have a consistent backbone (a sequence of repeating  $N - C_{\alpha} - C$ , where  $C_{\alpha}$  is the centrally located carbon in the amino acid residue) and a finite set of amino acids, synthetic polymers boast a limitless design space to draw their repeat units and backbones from [1, 2]. Additionally, proteins and molecules are aperiodic and non-periodic, respectively. In combination with the aforementioned challenges, polymer structure datasets from MD or DFT have only recently been standardized and have not seen the scale required for generative modeling [12]. Moreover, past work [27] in general may overlook the need of representing chain level [12], amorphous [28, 5], and network systems [29], in simulations using periodic boundary conditions.

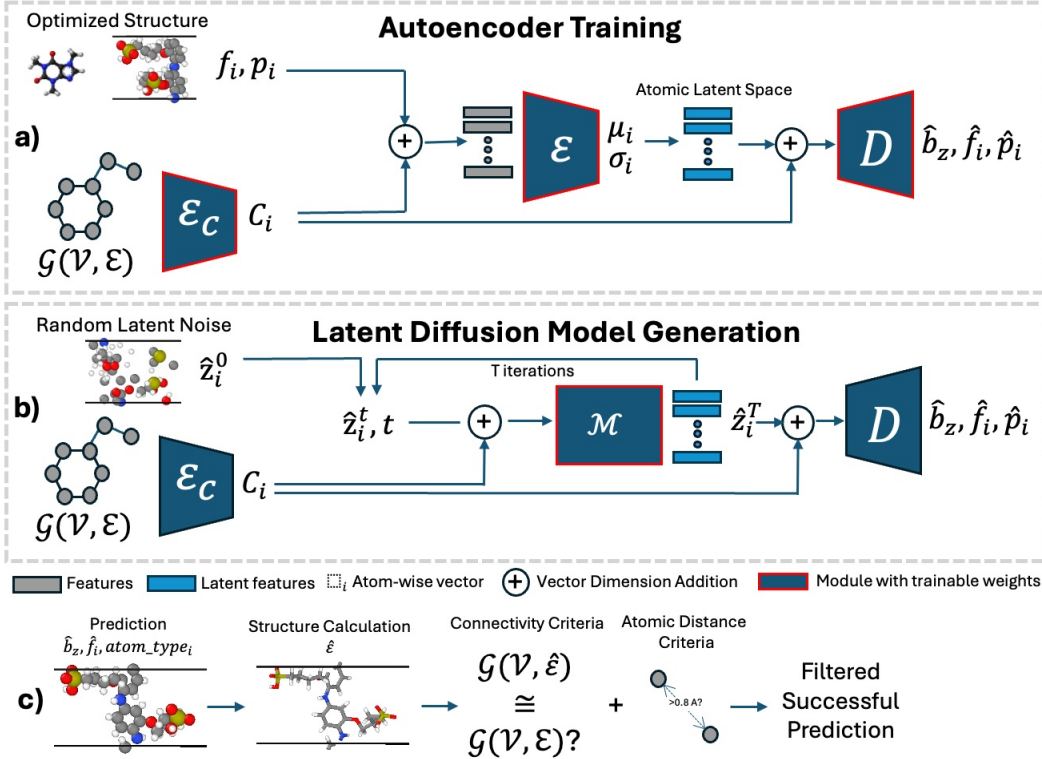


Figure 2: The training and generation process for polyGen. a) First, an autoencoder with conditional encoder  $\mathcal{E}_C$ , encoder  $\mathcal{E}$ , and decoder  $\mathcal{D}$  is trained to learn an atom-wise latent space by reconstructing the system as a bounding box  $\hat{b}_z$ , fractional coordinates  $\hat{f}_i$ , and cartesian coordinates  $\hat{p}_i$ . In this process, an atom-wise conditioning  $C_i$  is learned. b) The diffusion model  $\mathcal{M}$  is trained within this latent space, iteratively denoising a gaussian random latent  $\hat{z}_i^0$  into a new distribution  $\hat{z}_i^T$  that is likely a valid polymer conformation. c) During post-generation filtering, a structure is calculated from the predicted positions, and can be used if connectivity and bonding are preserved.

The complexity of polymer design and representation, combined with limited available data, explains why generative models for polymers have remained largely unexplored until now. We introduce polyGen (Figure 2), the first latent diffusion model specifically designed to generate periodic and stochastic polymeric structures. We build upon latent diffusion frameworks for materials generation such as All-Atom DiT [30]. Our problem and approach are modified to predict an ensemble of low-energy polymer conformations conditioned on a specified repeat unit with prescribed atomic connectivities rather than performing unconstrained de novo structure generation. Our method leverages a molecular encoding that captures atomic connectivity, which is used as a conditioning signal throughout the model architecture. We adopt a latent diffusion strategy over joint diffusion methods such as DiffCSP [18] or molecular generation methods in Cartesian space [23] due to the strong coupling between atomic positions and box dimensions imposed by polymer connectivity constraints. We augment our dataset with smaller structures from DFT-optimized molecules, demonstrating improved polymer structure prediction capabilities owing to the shared weights of a dataset invariant encoder and decoder, and a shared latent space. This work culminates in a learning framework that can generate ensembles of realistic polymer chain conformations. To benchmark the quality of these conformations, we introduce rigorous evaluation criteria grounded in first principles—standards that, to our knowledge, have not yet been applied in the context of materials generation. This application represents a novel proof-of-concept to predict atomic-level synthetic polymer conformations while accounting for their intrinsic flexibility and the distribution of plausible structures.

## 2 Results

### 2.1 Dataset and Evaluation Metrics

The main dataset, polyChainStructures, consists of 3855 DFT-optimized infinite polymer chain structures, with a maximum of 208 atoms, including hydrogens. Further details of this already open-sourced dataset, as well as DFT methods can be found in [12]. We use a 3084/386/385 (train/validation/test) split for the polyChainStructures dataset. The QM9 dataset, which contains DFT-optimized small-molecule conformations, is used to augment the training, allowing the models to learn local patterns from molecular structures. We use the train set from QM9 [25] which is a size of 100K molecules. We acknowledge the presence of larger molecular datasets (i.e., GEOM) that could be used to further augment our model’s learning [31]. However, from a structural perspective, the conformational behavior of non-zero temperature molecules found in GEOM differs significantly from the idealized infinite chains at 0K modeled in this work.

We benchmark polymer structure prediction on our polyChainStructures test set with our method. Unlike crystals, polymers are amorphous and can adopt many valid low-energy conformations, making conventional structure matching [32] unsuitable. Molecule generation is also evaluated with root mean squared distance after rotational alignment, but this doesn’t account for conformational variability experienced by infinite chains.

To this end, we compare the predicted conformations against the DFT-optimized structures by examining distributions over bond lengths, bond angles, and dihedrals. We quantify similarity using the forward Kullback–Leibler (KL) divergence from the predicted distribution to the ground truth. The task is to generate a distribution of plausible polymer conformations and assess the likelihood that the DFT-optimized structure could have been drawn from this predicted distribution. For a set of predicted quantities  $Q_{\text{pred}}$  we match it to the set of DFT predicted quantities  $Q_{\text{DFT}}$  with

$$\mathcal{L}_{\text{KL}} = D_{\text{KL}}(Q_{\text{DFT}} \parallel Q_{\text{pred}}) = \int Q_{\text{DFT}}(z) \log \frac{Q_{\text{DFT}}(z)}{Q_{\text{pred}}(z)} dz \quad (1)$$

In practice, we do this over a discrete set of buckets where  $dz$  is 0.001 of the predefined ranges of the quantities, which could be bond lengths (0.9 to 2.0), angles (0 to 180), or dihedrals (0 to 360).

### 2.2 Structure Matching Results

We find that our model is capable of predicting polymer structures that closely match the linear chain structure calculated by DFT. To provide context to our rationale, Figure 3 shows examples of predicted polymers compared to the ground truth of the dataset. In Figure 3a-d we see the capabilities of generating systems with qualitatively similar structures after filtering. We also provide examples of errors that are caught by our filtering. In Figure 3a and c, we see examples of carbon atoms incorrectly predicted within a supposedly aromatic ring in the backbone, which lead to incorrect connectivity. Despite Figure 3b being a failed structure, this error can easily be fixed with an energy minimization or a heuristic-based increasing of the C-H bond, demonstrating the efficacy of the remaining generation and the stringent nature of the generation filter. Also, the complexity of these structures should be noted, given chain size, branching, and the number of rings present.

To quantify structural similarity, we compare bond length, triplet angle, and dihedral angle distributions for specific atomic species. Like X-ray diffraction analysis, predicted structures should exhibit peaks comparable to optimized structures. On the right side of Figure 3, we observe variable distributions—most predictions cluster near optimized peaks with some outliers. The forward KL divergences establish benchmarks for acceptable "matches" in bond lengths, angles, and dihedrals.

We find that our approach can find relative trends in the majority of bond lengths, but lacks precision. For example, the predicted C-O bonds in Figure 3a and C-C bonds in Figure 3d show 2 peaks for single and double bonds, with noisy predictions scattered by at least 0.1 Å around these peaks. Additionally, the distribution of the predicted C-S bonds in Figure 3c includes an appropriate higher bond length, but with a much higher dispersity of predictions which results in a high KL divergence of 3.08. A similar example is found for the C-N single bond in Figure 3b. This makes it evident that generation is precise to the order of Å, but not on the scale of picometers. Precision on the level

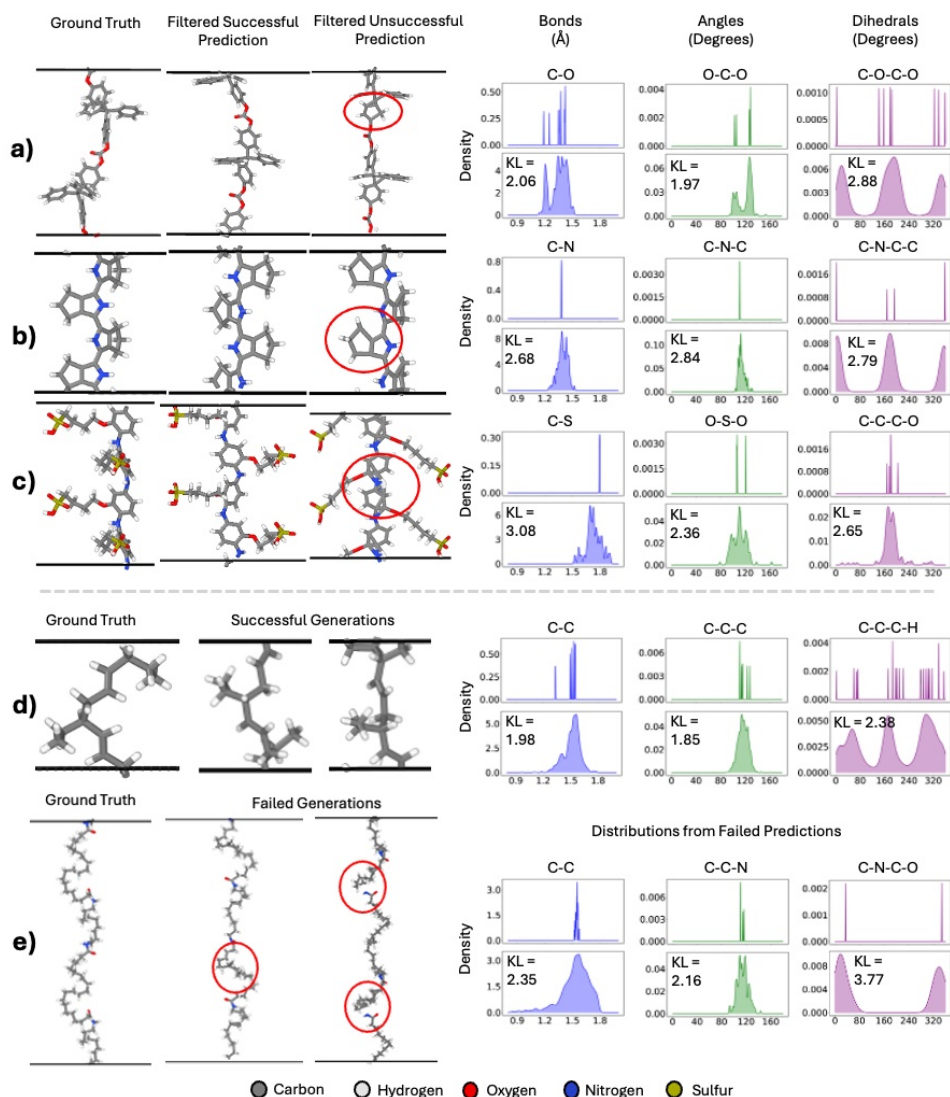


Figure 3: Visual samples from 100 generations per polymer type. Each row displays examples from a single polymer, accompanied by corresponding ground truth distributions (top) and model-predicted distributions (bottom) of molecular bonds, angles, and dihedrals for that polymer. For a-c, the ground truth, a successfully generated sample, and an unsuccessful sample are provided. The unsuccessful samples highlight the errors that caused the incorrect connectivity. Note that the structures for b) and c) are replicated along the z-axis for visual clarity of the structure. d) An example of a simple repeat unit for which no predictions fail. e) An example of the largest structure in the test set, with 208 atoms, for which all generations fail.

of picometers will be necessary to properly distinguish between bond types before our approach is scaled to larger system sizes.

Angles and dihedrals might vary based on the conformation. We find that the nature of these distributions also matches the ground truth peaks, especially the O-C-O, O-S-O, and C-C-C bonds in Figure 3a, c and d respectively. The dihedral distributions can be used to validate the prediction of correct local structures in the polymer. For example, the C-N-C-C dihedrals in Figure 3b validate the feasible prediction of the nitrogen containing 5-membered ring in the backbone. In Figure 3c, the C-C-C-O dihedral on the long branch is predicted similarly in a majority of cases based on the probability density, but has a wider extraneous variability of predictions. This conveys the challenges in predicting structures for branched polymers.

Figure 3e shows the failed predictions for the largest system across the train, validation, and test datasets, which is in our test set. Since none of the generations pass our filter, we show distributions from all failed predictions. We see the wide distribution of C-C bonds which extends to  $<1.0 \text{ \AA}$  due to the irregular placement of C atoms in these failed structures. A similar occurrence can be seen in the predicted C-C-N angle, which matches the peak of the DFT optimized structure, but with a larger distribution of noisy peaks. These results place a clear limit on the size of system due to the training dataset constraints, demonstrating the challenges of predicting feasible structures for larger polymer repeat units.

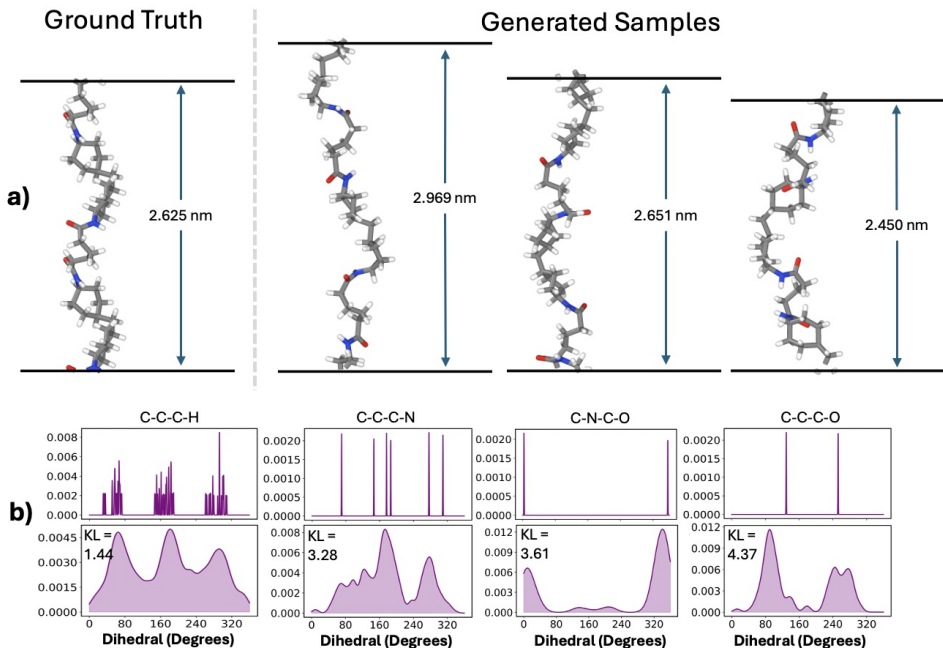


Figure 4: a) Demonstration of diverse structures generated from polyGen for the same repeat unit, compared to the ground truth structure. b) The ground truth dihedrals (top) compared to the distributions of the full generated ensemble (bottom) along with the KL Divergence. For reference, the structures are generated from the polymer repeat unit in Figure 1.

### 2.3 Prediction of Diverse Samples

As highlighted earlier, polymer structures do not reside in one fixed conformation but occur as an ensemble of minimized conformations, even close to 0 K. Our training dataset contains only 1 conformational example out of the potential ones, because the generation of these ensembles is costly. A useful generation model would produce a diverse ensemble of conformations representative of many possible low-energy states. In Figure 4b, despite the lack of per-polymer distribution in our dataset, polyGen can generate an ensemble of diverse structures with variable repeat unit lengths. Moreover, these samples pass the post-generation filtering and remain consistent with structural features in the DFT ground truth, as seen in the KL Divergences in Figure 4b.

### 2.4 Overall Results

Following previous works, we also see that joint training on multiple DFT datasets can improve model performance [30, 16]. In this section, we show the specific areas in which the inclusion of the QM9 dataset can benefit the generation of polymer structures by comparing the joint dataset approach with a model fully trained on just the polyChainStructures dataset. Figure 6 shows the overall KL divergences for bond lengths, angle lengths, and dihedrals, and comparison of predicted z-height. The inclusion of the QM9 dataset improves predictions on the local levels of polymer chains, as the KL divergences of bonds and angles decrease by 41.0% and 29.0%, respectively, upon the addition of the QM9 dataset. Larger features, such as dihedral angles and the z-height show

limited improvement, with dihedrals improving by 16.1%. This is likely because small molecules do not provide any insight into the macrostructural properties of polymers. Overall, we find that 36.1% of the generated structures by the jointly trained model pass our filtering, whereas 27.4% samples are generated correctly when using only the polyChainStructures dataset for training.

As highlighted in Figure 6d and discussed in Section 2.3, we expect some variability in the prediction of the z-height of the polymer chain. Despite this, we can achieve an  $r^2$  score of 0.822 between the predicted and DFT heights, meaning that the model can differentiate between dense vs. sparsely packed structures. Additionally, we see a larger standard deviation and error in predictions for larger repeat units ( $> 10 \text{ \AA}$ ), because these repeat units may show more flexibility. Figure 6E also shows a notable trend in the difficulty of generating feasible structures as system size increases. Most generated systems with  $< 25$  atoms show success rates  $> 0.5$ . For system sizes greater than 150 atoms, we find errors in connectivity for all generated systems, similar to the examples shown in Figure 3E. Intuitively, it would also seem that complex polymeric structures would be more difficult to generate. To this end, we also compare these metrics with the Synthetic Accessibility (SA) in Supplementary Information A. We see loose correlations with KL divergences of bond length, angles, and dihedrals with the SA score, but the ratio of successful generations of a polymer do not have a strong correlation with the SA score. Therefore, generation success could be independent from SA score and more reliant on the system size.

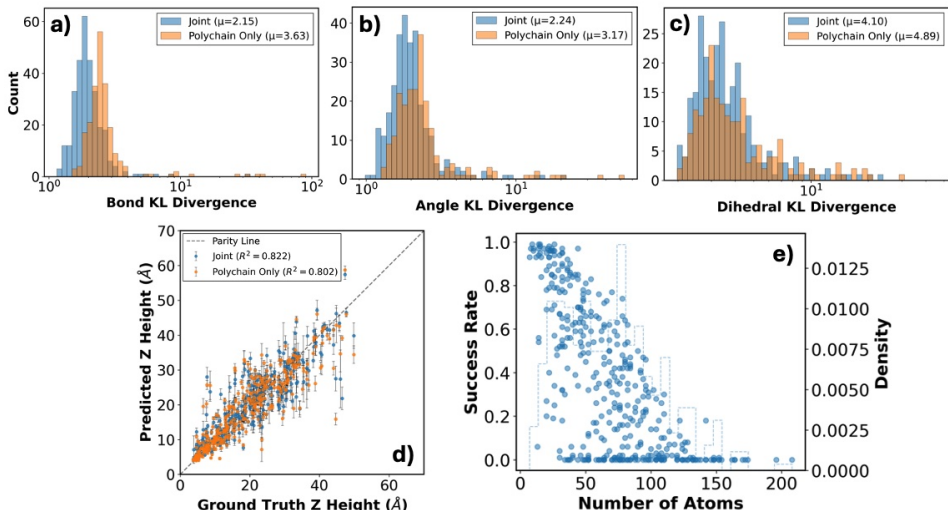


Figure 5: KL Divergences of Joint training vs. polyChainStructures only for a) Bonds b) Angles and c) Dihedrals. d) The comparison of z-height prediction vs the DFT ground truth. e) The success rate of filtering as a function of the atom count of the system. A histogram in the back provides the distributions of atom counts found in the test dataset, with the density provided on the right y-axis.

Methodologically, increasing the diffusion transformer’s size [30] and addressing the sign-invariance of Laplacian eigenvector positional encodings—using techniques such as SignNet [33, 34]—could further enhance the framework’s performance especially with larger systems.

### 3 Discussion

In this study, we introduce a solution to the problem of atomic-level polymer structure generation—given only the atomic connectivity of a repeat unit (i.e. SMILES), polyGen can generate an ensemble of realistic 3D structures of synthetic polymers. Results demonstrate that polyGen effectively generates structures with bond lengths, angles, and dihedral distributions that align well with ground truth structures. The model also successfully generates valid conformations for complex features like aromatic backbones and branches while correlating repeat unit chemistry with structural properties, such as repeat unit length. These initial results are particularly promising considering our polymer structure dataset optimized with Density Functional Theory contains only 3855 systems. We also investigate the limitations and demonstrate the need for stringent benchmarking of future

polymer structure generation techniques. While capturing relative trends in structure, the model lacks precision at the picometer scale needed to definitively distinguish between bond types. Performance degrades significantly for larger polymeric systems, likely due to dataset constraints. Finally, the consistency of feasible generation needs to be improved. Given the successes of this proof-of-concept, future work will focus on expanding the training dataset to include larger polymer systems, incorporating additional physics-informed constraints, and exploring hybrid approaches that combine latent diffusion with molecular dynamics simulations. Addressing these challenges could transform polyGen into an invaluable tool for computational materials science, accelerating the discovery of novel polymeric materials across numerous applications.

## 4 Methods

polyGen consists of three phases, a 0D conditioning on the molecular graph of the desired polymer repeat unit chemical structure, a variational autoencoder for structure (Figure 2a), and a latent diffusion module (Figure 2b). Overall, we choose an architecture that does not include any equivariance or inductive biases, following the sentiment of recent works [30, 21] where data scale and augmentation can be a path to learning these more efficiently.

### 4.1 Polymer Structure Specification

Several previous works have learned structural and chemical representations of periodic materials, which include fractional coordinates, unit cell lengths, and lattice angles. For single polymer chain structures, we take a modified approach. Because of their complexity, training set structures are optimized using DFT with a periodic orthogonal box where the chain is continuous through the  $z$  axis. The width of the box is needed to encapsulate side chains/branched structures and are made large enough to isolate the single chain during optimization.

We note that the  $x$  and  $y$  axis are not entirely polymer structure dependent. Including these as prediction variables is an overparameterization, and does not contribute much information. Therefore, we fix the  $x$  and  $y$  of the box to a  $55 \text{ \AA} \times 55 \text{ \AA}$  box, and define the system by the  $z$  height of the box,  $b_z$ . In theory, this quantity is a proxy for the system’s density (which is also stochastic, depending on the specific sampled configurations). Atomic positions are provided as fractional coordinates within this orthogonal bounding box.

### 4.2 Graph Conditioning

The generation of polymer structures begins with a minimal representation of atomic connectivity, typically provided in the form of a SMILES string. This string is converted into a molecular graph: periodic for polymers and non-periodic for small molecules. To extract a universal atom-wise representation, denoted as  $C_i$ , we apply a graph conditioning module that encodes the molecular connectivity. As illustrated in Figure 2a and b,  $C_i$  serves as contextual input to the encoder, decoder, and diffusion modules. The graph conditioning module is implemented using a graph interaction network, similar to [35], which captures local chemical environments by modeling interactions between different atom and bond types. Importantly, the same network weights are used across all datasets and connectivity types, facilitating effective transfer learning and generalization across chemical spaces.

Given a graph  $\mathcal{G} = (\mathcal{V}, \mathcal{E})$ , each node  $i \in \mathcal{V}$  is associated with an atom type and positional encodings, and each edge  $(i, j) \in \mathcal{E}$  is associated with a bond type. The initial node and edge embeddings are computed as:

$$\begin{aligned} \mathbf{h}_i^{(0)} &= \text{Embed}(\text{atom\_type}_i) \\ \mathbf{e}_{ij}^{(0)} &= \text{Embed}(\text{bond\_type}_{ij}) \\ \mathbf{h}_i^{(0)} &= \text{MLP}([\mathbf{h}_i^{(0)}; \mathbf{r}_i^{\text{RW}}; \mathbf{r}_i^{\text{Lap}}]) \end{aligned} \tag{2}$$

For each layer  $l = 1, \dots, L$ :

#### Edge Update:

$$\mathbf{e}_{ij}^{(l)} = \mathbf{e}_{ij}^{(l-1)} \mathbf{W}_e + f_e^{(l)}(\text{LN}([\mathbf{e}_{ij}^{(l-1)}; \mathbf{h}_i^{(l-1)}; \mathbf{h}_j^{(l-1)}])) \tag{3}$$

**Node Update:**

$$\begin{aligned} \mathbf{m}_i^{(l)} &= \sum_{j \in \mathcal{N}(i)} \mathbf{e}_{ij}^{(l)} \\ \mathbf{h}_i^{(l)} &= \mathbf{h}_i^{(l-1)} \mathbf{W}_v + f_v^{(l)}(\text{LN}([\mathbf{m}_i^{(l)}; \mathbf{h}_i^{(l-1)}])) \end{aligned} \tag{4}$$

**Global Pooling and Final Representation:**

$$\begin{aligned} \mathbf{g} &= \sum_{i \in \mathcal{V}} \mathbf{h}_i^{(L)} \\ C_i &= f_f^{(l)}([\mathbf{g}; \mathbf{h}_i^{(L)}]) \end{aligned} \tag{5}$$

where  $f_e^{(l)}$ ,  $f_v^{(l)}$ ,  $f_f^{(l)}$  are MLPs, LN is layer normalization,  $\mathbf{r}_i^{\text{RW}}$  is a random walk positional encoding [36] of size 16 and  $\mathbf{r}_i^{\text{Lap}}$  is a Laplacian positional encoding [37, 38] of size 2. We use  $L = 4$  to capture local interactions of an atom 1 "hop" away from its furthest dihedral. The global pooling prior to embedding into token dimension is done so that atomic-level information is taken with global system information.

The encoder, decoder, and diffusion modules are all transformers, which typically require a positional encoding to identify token ordering and condition the self-attention weights. Similar to contemporary graph transformer methods,  $C_i$  communicates this by providing embeddings calculated from  $\mathbf{r}_i^{\text{RW}}$  and  $\mathbf{r}_i^{\text{Lap}}$  [34].

**4.3 Structural Variational AutoEncoder**

The next step is to learn a way to combine all aspects of a polymer system, such as monomer chemistry, fractional coordinates, and the bounding box, into a joint space. This space should also allow the fusion of information from small molecules or other systems to enhance learning. We employ a VAE to create unified atom-wise latent representation that contains structural details for small molecules and polymers,  $\mathcal{Z} \in \mathcal{R}^d$  where  $d$  is a latent dimension. The VAE is based on traditional graph VAEs, including an encoder  $\mathcal{E}$  and a decoder  $\mathcal{D}$  operating atom-wise.

The structure of the molecule/polymer is given through a concatenated vector of fractional coordinates  $f_i$  and Cartesian positions  $p_i$ . For a polymer structure, both the  $f_i$  and scaled  $p_i$  according to the bounding box are provided. This forces the VAE to learn and reconstruct the relationship between the Cartesian positions, fractional coordinates, and the bounding box. For non-periodic molecules,  $p_i$  is provided and  $f_i = \emptyset$ , which allows periodic and non-periodic materials to share the same latent space, similar to [30]. The atom-wise latent space is then calculated along with the  $C_i$ .

$$\mu_i, \sigma_i = \mathcal{E}(f_i, p_i, C_i) \tag{6}$$

$$\mathcal{Z}_i \sim \mathcal{N}(\mu_i, \sigma_i) \tag{7}$$

The decoder then produces a structure from  $\mathcal{Z}$ ,

$$\hat{f}_i, \hat{p}_i, \hat{b}_z = \mathcal{D}(\mathcal{Z}, C_i) \tag{8}$$

where  $\hat{f}_i$  is the predicted fractional coordinates,  $\hat{p}_i$  is the predicted cartesian coordinates, and  $\hat{b}_z$  is the  $z$  direction height of the bounding box. The loss on the decoder is used to optimize the model

$$\begin{aligned} \mathcal{L}_{\text{total}} &= \langle w_{\text{bbox}} \cdot \mathcal{L}_{\text{bbox}} \rangle + \langle w_{\text{frac\_coords}} \cdot \mathcal{L}_{\text{frac\_coords}} \rangle + \langle w_{\text{pos}} \cdot \mathcal{L}_{\text{pos}} \rangle \\ &+ \langle w_{\text{kl}} \cdot \mathcal{L}_{\text{kl}} \rangle + \langle w_{\text{bond}} \cdot \mathcal{L}_{\text{bond}} \rangle + \langle w_{\text{angle}} \cdot \mathcal{L}_{\text{angle}} \rangle + \langle w_{\text{dihedral}} \cdot \mathcal{L}_{\text{dihedral}} \rangle \end{aligned} \tag{9}$$

Where the reconstruction terms are defined as:

$$\begin{aligned} \mathcal{L}_{\text{bbox}} &= \text{MSE}(\hat{b}_z, b_z / (10 * \sqrt[3]{N})) \\ \mathcal{L}_{\text{frac\_coords}} &= \frac{1}{d} \sum_i \text{MSE}(\hat{f}_i, f_i) \\ \mathcal{L}_{\text{pos}} &= \frac{1}{d} \sum_i \text{MSE}((\hat{p}_i - \langle \hat{p} \rangle), (p_i - \langle p \rangle)) \\ \mathcal{L}_{\text{kl}} &= \text{KL}(q_\phi(z|x) \| p(z)) \end{aligned}$$

And the structural loss terms from are:

$$\begin{aligned} \mathcal{L}_{\text{bond}} &= \text{MSE}(d_{ij}, \hat{d}_{ij}) \\ \mathcal{L}_{\text{angle}} &= \text{MSE}(\angle_{ijk}, \hat{\angle}_{ijk}) \\ \mathcal{L}_{\text{dihedral}} &= (\Delta_{\text{periodic}}(\tau_{ijkl}, \hat{\tau}_{ijkl}))^2 \end{aligned}$$

Where:

- $d_{ij}$  = bond length between atoms  $i$  and  $j$  computed with true coordinates and box
- $\hat{d}_{ij}$  = bond length between atoms  $i$  and  $j$  computed with predicted coordinates and box
- $\angle_{ijk}$  = angle between bonded atoms  $i$ - $j$ - $k$  computed with true coordinates
- $\hat{\angle}_{ijk}$  = angle between bonded atoms  $i$ - $j$ - $k$  computed with predicted coordinates
- $\tau_{ijkl}$  = dihedral angle formed by atoms  $i$ - $j$ - $k$ - $l$  computed with true coordinates
- $\hat{\tau}_{ijkl}$  = dihedral angle formed by atoms  $i$ - $j$ - $k$ - $l$  computed with predicted coordinates
- $\Delta_{\text{periodic}}$  = periodic difference within  $0$ - $2\pi$  radians
- $N$  = number of atoms in the system

The inclusion of the structural loss is to help the VAE optimize to decode structures that are structurally similar to the target, even if the positions may be slightly different than the target. Similar approaches for enforcing local atomic relations are utilized in works concerning biological polymer structures [21, 39]. Final model hyperparameters are provided in Supplementary Information C.

#### 4.4 Diffusion Transformer

Now that a joint latent space is learned, we require a way to find suitable structures for new polymer chemistries. We use a DiT architecture for our generative model  $\mathcal{M}$ , operating within the latent space  $\mathcal{Z}$  learned by the VAE. We use a similar DiT architecture as ADiT [30], however the previous work uses sinusoidal positional encodings for atomic tokens, which make it difficult for unordered atomic representations. In our case, we want to preserve the permutation invariant qualities of a GNN, so we use the positional encoded features and interactions in  $C_i$  to provide positional information relative to other atoms in the system.

Our denoiser is implemented through a gaussian flow matching approach, which is equivalent to denoising diffusion as one can be derived from the other [40, 30]. We start by encoding a DFT optimized structure into the latent space, using Equation 7, to get  $\mathcal{Z}_1$ . Similar to other latent diffusion/flow matching works we denoise from zero-centered random noise  $\mathcal{Z}_0 \sim \mathcal{N}(0, 1)$  at  $t = 0$  to  $\mathcal{Z}_1$  at  $t = 1$  [30]. To train the transformer, we provide it with an interpolated sample  $\mathcal{Z}_t$  at a random timestep  $t \sim \mathcal{U}(0, 1)$ ,

$$\mathcal{Z}_t = (1 - t)\mathcal{Z}_0 + t\mathcal{Z}_1 \tag{10}$$

We can pose the learning problem as the linear ordinary differential equation (ODE),

$$u_t = \dot{\mathcal{Z}}(\mathcal{Z}_t) = \frac{\mathcal{Z}_1 - \mathcal{Z}_t}{1 - t} \tag{11}$$

The final prediction task for the graph diffusion model is defined as,

$$\begin{aligned} \hat{\mathcal{Z}}_1 &= \mathcal{M}(\mathcal{Z}_t, \mathcal{Z}_{\text{sc}}, t, C_i, S) \\ \hat{u}_t &= \frac{\hat{\mathcal{Z}}_1 - \mathcal{Z}_t}{1 - t}, \end{aligned}$$

where  $S$  is an embedding that represents the dataset used during generation. This is used exclusively during joint training. Only the embedding for the polyChainStructures dataset is used during inference.  $\mathcal{Z}_{\text{sc}}$  denotes a self-conditioning input, which corresponds to a previous prediction of  $\hat{\mathcal{Z}}_1$ . Self-conditioning has been shown to improve performance in autoregressive molecular generation tasks [41, 30].

In our training implementation, we follow a two-pass approach:

- In the first pass, we predict  $\hat{\mathcal{Z}}_1$  using no self-conditioning, i.e.,  $\mathcal{Z}_{\text{sc}} = \emptyset$ .
- In the second pass, the predicted  $\hat{\mathcal{Z}}_1$  is fed back as  $\mathcal{Z}_{\text{sc}}$  to provide additional context for refinement.

To regularize the model and prevent over-reliance on self-conditioning, we follow standard practice and randomly drop the self-conditioning input during training [41, 30]. Specifically, with probability 0.5, we set  $\mathcal{Z}_{\text{sc}} = \emptyset$ .

The training objective is defined as the atom-wise mean squared error between  $\hat{u}_t^{(i)}$  and  $u_t^{(i)}$  for  $N$  atoms in a system:

$$\mathcal{L}_{\mathcal{G}} = \frac{1}{N} \sum_{i=1}^N \left\| u_t^{(i)} - \hat{u}_t^{(i)} \right\|^2 \quad (12)$$

$$= \frac{1}{N} \sum_{i=1}^N \left\| \frac{\mathcal{Z}_1^{(i)} - \mathcal{Z}_t^{(i)}}{1-t} - \frac{\hat{\mathcal{Z}}_1^{(i)} - \mathcal{Z}_t^{(i)}}{1-t} \right\|^2 \quad (13)$$

$$= \frac{1}{(1-t)^2} \cdot \frac{1}{N} \sum_{i=1}^N \left\| \mathcal{Z}_1^{(i)} - \hat{\mathcal{Z}}_1^{(i)} \right\|^2 \quad (14)$$

To prevent numerical instability in the loss function calculation, we clip the value of  $t$  to 0.9, in accordance with previous work [30].

During inference, we sample an initial latent  $\mathcal{Z}_0 \sim \mathcal{N}(0, I)$  and iteratively denoise it using  $T$  steps of Euler integration:

$$\mathcal{Z}_{t+\Delta t} = \mathcal{Z}_t + \Delta t \hat{u}_t,$$

where  $\Delta t = 1.0/T$ . This process generates a final conformation  $\hat{\mathcal{Z}}_1$ , which is decoded into a novel 3D atomic system using  $\mathcal{D}$ . We compare generation hyperparameters in Supplementary Information B, and show final model hyperparameters in Supplementary Information C.

#### 4.5 Post-Generation Filtering

Often, sampling from a flow matching or diffusion model can lead to unphysical generations. In Figure 2, we show stringent post-generation filtering test. This is generalizable and not dependent on the final ground-truth structure. First, we take the final predicted system ( $\text{atom\_type}_i, \hat{b}_z, \hat{f}_i$ ) and use the Cartesian distances between atoms to calculate the predicted structure based on estimates of bond lengths between different atoms in organic structures. The connectivity of the predicted structure is represented as the predicted graph  $\hat{\mathcal{G}} = (\mathcal{V}, \hat{\mathcal{E}})$ . As a first filter, we test whether the ground truth graph  $\mathcal{G}$  and the predicted graph  $\hat{\mathcal{G}}$  are isomorphic, i.e., whether  $\mathcal{G} \cong \hat{\mathcal{G}}$ . If this test fails, this means that there are atoms that should be bonded but are predicted too far from one another or atoms are too close to each other. The next filter simply looks at the calculated bond lengths based on  $\hat{\mathcal{E}}$  and filters out the structures containing bond lengths  $< 0.8$ . Samples that pass this filtering criteria will be "successful" and those that don't are "unsuccessful." However, a successful prediction of connectivity doesn't guarantee an accurate 3D structure, and the successful samples are evaluated against the optimized 3D structures in Section 2.

#### 4.6 Machine Learning Techniques

Our main polymer DFT dataset, polyChainStructures (elaborated in Section 2.1), and the QM9 dataset are imbalanced, with the latter training set being  $\approx 33x$  larger. To handle this we upsample

the polyChainStructures data by 30x per epoch. During training for the polychain dataset only, this upsampling ratio is held the same for comparison, so that both models see the same amount of polyChainStructures data per epoch. To learn equivariance, we randomly rotate and translate the systems at every training step for both the VAE and the DiT.

The autoencoder models were trained for 300 epochs, and the highest-performing validation checkpoint was taken. The diffusion models were trained for a maximum of 500 epochs.

## 5 Data Availability

The dataset used in this study is available on the Ramprasad group’s computational knowledge-base, Khazana (<https://khazana.gatech.edu/dataset>).

## 6 Code Availability

The code used for this work will be made publicly available upon publication on the Ramprasad group’s github (<https://github.com/Ramprasad-Group>)

## 7 Acknowledgements

This work was financially supported by the Office of Naval Research (ONR) through Grant N00014-21-1-2258 and the National Science Foundation (NSF) DMREF Grant 2323695. A.J. acknowledges S. Shukla, A. Savit, H. Sahu, H. Tran, and R. Gurnani for valuable discussions.

## 8 Author Contributions

A.J. is the main architect of the models and wrote the paper. R.R. conceived the project and guided the work and the previous project for dataset generation.

## 9 Competing Interests

R.R. is a founder of Matmerize, Inc., a company specializing in materials informatics software and services. The other authors have no conflicts of interest to declare.

## References

- [1] Huan Tran, Rishi Gurnani, Chiho Kim, Ghanshyam Pilania, Ha-Kyung Kwon, Ryan P Lively, and Rampi Ramprasad. Design of functional and sustainable polymers assisted by artificial intelligence. *Nature Reviews Materials*, pages 1–21, 2024.
- [2] Rohit Batra, Le Song, and Rampi Ramprasad. Emerging materials intelligence ecosystems propelled by machine learning. *Nature Reviews Materials*, 6(8):655–678, 2021.
- [3] Shivank S Shukla, Christopher Kuenneth, and Rampi Ramprasad. Polymer informatics beyond homopolymers. *arXiv preprint arXiv:2303.12938*, 2023.
- [4] Rishi Gurnani, Stuti Shukla, Deepak Kamal, Chao Wu, Jing Hao, Christopher Kuenneth, Pritish Aklujkar, Ashish Khomane, Robert Daniels, Ajinkya A Deshmukh, et al. Ai-assisted discovery of high-temperature dielectrics for energy storage. *Nature Communications*, 15(1):6107, 2024.
- [5] Brandon K Phan, Kuan-Hsuan Shen, Rishi Gurnani, Huan Tran, Ryan Lively, and Rampi Ramprasad. Gas permeability, diffusivity, and solubility in polymers: Simulation-experiment data fusion and multi-task machine learning. *npj Computational Materials*, 10(1):186, 2024.
- [6] Lihua Chen, Ghanshyam Pilania, Rohit Batra, Tran Doan Huan, Chiho Kim, Christopher Kuenneth, and Rampi Ramprasad. Polymer informatics: Current status and critical next steps. *Materials Science and Engineering: R: Reports*, 144:100595, 2021.
- [7] Huan Doan Tran, Chiho Kim, Lihua Chen, Anand Chandrasekaran, Rohit Batra, Shruti Venkatram, Deepak Kamal, Jordan P Lightstone, Rishi Gurnani, Pranav Shetty, et al. Machine-learning predictions of polymer properties with polymer genome. *Journal of Applied Physics*, 128(17):171104, 2020.

- [8] Rishi Gurnani, Christopher Kuenneth, Aubrey Toland, and Rampi Ramprasad. Polymer informatics at scale with multitask graph neural networks. *Chemistry of Materials*, 35(4):1560–1567, 2023.
- [9] Joseph Kern, Yongliang Su, Will Gutekunst, and Rampi Ramprasad. An informatics framework for the design of sustainable, chemically recyclable, synthetically-accessible and durable polymers. *arXiv preprint arXiv:2409.15354*, 2024.
- [10] Joseph Kern, Lihua Chen, Chiho Kim, and Rampi Ramprasad. Design of polymers for energy storage capacitors using machine learning and evolutionary algorithms. *Journal of Materials Science*, 56:19623–19635, 2021.
- [11] Rohit Batra, Hanjun Dai, Tran Doan Huan, Lihua Chen, Chiho Kim, Will R Gutekunst, Le Song, and Rampi Ramprasad. Polymers for extreme conditions designed using syntax-directed variational autoencoders. *Chemistry of Materials*, 32(24):10489–10500, 2020.
- [12] Tran Doan Huan and Rampi Ramprasad. Polymer structure prediction from first principles. *The Journal of Physical Chemistry Letters*, 11(15):5823–5829, 2020.
- [13] Hari Krishna Sahu, Kuan-Hsuan Shen, Joseph H Montoya, Huan Tran, and Rampi Ramprasad. Polymer structure predictor (psp): a python toolkit for predicting atomic-level structural models for a range of polymer geometries. *Journal of Chemical Theory and Computation*, 18(4):2737–2748, 2022.
- [14] Ling Yang, Zhilong Zhang, Yang Song, Shenda Hong, Runsheng Xu, Yue Zhao, Wentao Zhang, Bin Cui, and Ming-Hsuan Yang. Diffusion models: A comprehensive survey of methods and applications. *ACM Computing Surveys*, 56(4):1–39, 2023.
- [15] Yaron Lipman, Ricky TQ Chen, Heli Ben-Hamu, Maximilian Nickel, and Matt Le. Flow matching for generative modeling. *arXiv preprint arXiv:2210.02747*, 2022.
- [16] Richard Tran, Janice Lan, Muhammed Shuaibi, Brandon M Wood, Siddharth Goyal, Abhishek Das, Javier Heras-Domingo, Adeesh Kolluru, Ammar Rizvi, Nima Shoghi, et al. The open catalyst 2022 (oc22) dataset and challenges for oxide electrocatalysts. *ACS Catalysis*, 13(5):3066–3084, 2023.
- [17] John Jumper, Richard Evans, Alexander Pritzel, Tim Green, Michael Figurnov, Olaf Ronneberger, Kathryn Tunyasuvunakool, Russ Bates, Augustin Židek, Anna Potapenko, et al. Highly accurate protein structure prediction with alphafold. *nature*, 596(7873):583–589, 2021.
- [18] Rui Jiao, Wenbing Huang, Peijia Lin, Jiaqi Han, Pin Chen, Yutong Lu, and Yang Liu. Crystal structure prediction by joint equivariant diffusion. *Advances in Neural Information Processing Systems*, 36:17464–17497, 2023.
- [19] Tian Xie, Xiang Fu, Octavian-Eugen Ganea, Regina Barzilay, and Tommi Jaakkola. Crystal diffusion variational autoencoder for periodic material generation. *arXiv preprint arXiv:2110.06197*, 2021.
- [20] Benjamin Kurt Miller, Ricky TQ Chen, Anuroop Sriram, and Brandon M Wood. Flowmm: Generating materials with riemannian flow matching. In *Forty-first International Conference on Machine Learning*, 2024.
- [21] Josh Abramson, Jonas Adler, Jack Dunger, Richard Evans, Tim Green, Alexander Pritzel, Olaf Ronneberger, Lindsay Willmore, Andrew J Ballard, Joshua Bambrick, et al. Accurate structure prediction of biomolecular interactions with alphafold 3. *Nature*, 630(8016):493–500, 2024.
- [22] Jeremy Wohlwend, Gabriele Corso, Saro Passaro, Mateo Reveiz, Ken Leidal, Wojtek Swiderski, Tally Portnoi, Itamar Chinn, Jacob Silterra, Tommi Jaakkola, et al. Boltz-1: Democratizing biomolecular interaction modeling. *bioRxiv*, pages 2024–11, 2024.
- [23] Majdi Hassan, Nikhil Shenoy, Jungyoon Lee, Hannes Stärk, Stephan Thaler, and Dominique Beaini. Et-flow: Equivariant flow-matching for molecular conformer generation. *Advances in Neural Information Processing Systems*, 37:128798–128824, 2024.
- [24] Minkai Xu, Alexander Powers, Ron Dror, Stefano Ermon, and Jure Leskovec. Geometric latent diffusion models for 3d molecule generation, 2023. URL <https://arxiv.org/abs/2305.01140>.
- [25] Zhenqin Wu, Bharath Ramsundar, Evan N Feinberg, Joseph Gomes, Caleb Geniesse, Aneesh S Pappu, Karl Leswing, and Vijay Pande. Moleculenet: a benchmark for molecular machine learning. *Chemical science*, 9(2):513–530, 2018.
- [26] Gabriele Corso, Hannes Stärk, Bowen Jing, Regina Barzilay, and Tommi Jaakkola. Diffdock: Diffusion steps, twists, and turns for molecular docking. *arXiv preprint arXiv:2210.01776*, 2022.
- [27] Fanmeng Wang, Wentao Guo, Qi Ou, Hongshuai Wang, Haitao Lin, Hongteng Xu, and Zhifeng Gao. Polyconf: Unlocking polymer conformation generation through hierarchical generative models. *arXiv preprint arXiv:2504.08859*, 2025.
- [28] Mohammad Atif Faiz Afzal, Andrea R Browning, Alexander Goldberg, Mathew D Halls, Jacob L Gavartin, Tsuguo Morisato, Thomas F Hughes, David J Giesen, and Joseph E Goose. High-throughput molecular dynamics simulations and validation of thermophysical properties of polymers for various applications. *ACS Applied Polymer Materials*, 3(2):620–630, 2020.

- [29] Mathilde Orselly, Julien Devey, Agathe Bouvet-Marchand, Alain Dequidt, Cédric Loubat, and Patrice Malfreyt. Molecular simulations of thermomechanical properties of epoxy-amine resins. *ACS omega*, 7(34):30040–30050, 2022.
- [30] Chaitanya K Joshi, Xiang Fu, Yi-Lun Liao, Vahe Gharakhanyan, Benjamin Kurt Miller, Anuroop Sriram, and Zachary W Ulissi. All-atom diffusion transformers: Unified generative modelling of molecules and materials. *arXiv preprint arXiv:2503.03965*, 2025.
- [31] Simon Axelrod and Rafael Gomez-Bombarelli. Geom, energy-annotated molecular conformations for property prediction and molecular generation. *Scientific Data*, 9(1):185, 2022.
- [32] Shyue Ping Ong, William Davidson Richards, Anubhav Jain, Geoffroy Hautier, Michael Kocher, Shreyas Cholia, Dan Gunter, Vincent L Chevrier, Kristin A Persson, and Gerbrand Ceder. Python materials genomics (pymatgen): A robust, open-source python library for materials analysis. *Computational Materials Science*, 68:314–319, 2013.
- [33] Derek Lim, Joshua Robinson, Lingxiao Zhao, Tess Smidt, Suvrit Sra, Haggai Maron, and Stefanie Jegelka. Sign and basis invariant networks for spectral graph representation learning. *arXiv preprint arXiv:2202.13013*, 2022.
- [34] Erxue Min, Runfa Chen, Yatao Bian, Tingyang Xu, Kangfei Zhao, Wenbing Huang, Peilin Zhao, Junzhou Huang, Sophia Ananiadou, and Yu Rong. Transformer for graphs: An overview from architecture perspective. *arXiv preprint arXiv:2202.08455*, 2022.
- [35] Peter Battaglia, Razvan Pascanu, Matthew Lai, Danilo Jimenez Rezende, et al. Interaction networks for learning about objects, relations and physics. *Advances in neural information processing systems*, 29, 2016.
- [36] Vijay Prakash Dwivedi, Anh Tuan Luu, Thomas Laurent, Yoshua Bengio, and Xavier Bresson. Graph neural networks with learnable structural and positional representations. *arXiv preprint arXiv:2110.07875*, 2021.
- [37] Vijay Prakash Dwivedi, Chaitanya K Joshi, Anh Tuan Luu, Thomas Laurent, Yoshua Bengio, and Xavier Bresson. Benchmarking graph neural networks. *Journal of Machine Learning Research*, 24(43):1–48, 2023.
- [38] Yuyang Wang, Ahmed A. A. Elhag, Navdeep Jaitly, Joshua M. Susskind, and Miguel Angel Bautista. Swallowing the bitter pill: Simplified scalable conformer generation. In *International Conference on Machine Learning*, 2023. URL <https://api.semanticscholar.org/CorpusID:265506007>.
- [39] Valerio Mariani, Marco Biasini, Alessandro Barbato, and Torsten Schwede. Iddt: a local superposition-free score for comparing protein structures and models using distance difference tests. *Bioinformatics*, 29(21):2722–2728, 2013.
- [40] Ruiqi Gao, Emiel Hoogetboom, Jonathan Heek, Valentin De Bortoli, Kevin P. Murphy, and Tim Salimans. Diffusion meets flow matching: Two sides of the same coin. 2024. URL <https://diffusionflow.github.io/>.
- [41] Hannes Stärk, Bowen Jing, Regina Barzilay, and Tommi Jaakkola. Harmonic self-conditioned flow matching for multi-ligand docking and binding site design. *arXiv preprint arXiv:2310.05764*, 2023.
- [42] Peter Ertl and Ansgar Schuffenhauer. Estimation of synthetic accessibility score of drug-like molecules based on molecular complexity and fragment contributions. *Journal of cheminformatics*, 1:1–11, 2009.
- [43] Tero Karras, Miika Aittala, Timo Aila, and Samuli Laine. Elucidating the design space of diffusion-based generative models. *Advances in neural information processing systems*, 35:26565–26577, 2022.

## 10 Appendix

### A Impact of SA Score on Generation

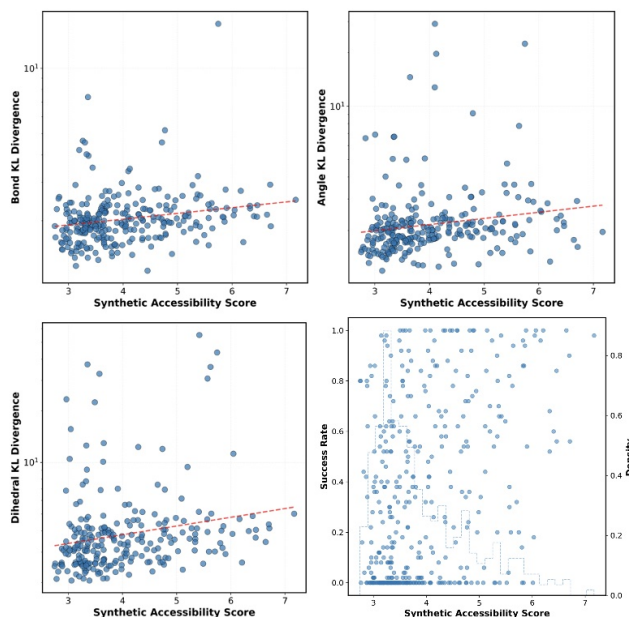


Figure 6: Impacts of Synthetic Accessibility (SA) score [42] on the quality of generation bonds, angles, dihedrals, and successes after filtering. The SA score is calculated through RDKit.

## B Generation Tuning

We present additional experiments on determining the quality of generation across changes to generation hyperparameters. In Figure 7a we find that increasing the number of the integration steps increases the the quality of generation until  $\sim 100$  steps. In Figure 7b, the percentage of successful samples increases slightly with the number of generated conformations per polymer chain, reaching saturation at 100 samples, which is a practical generation limit given our computational constraints.

Several works for autoregressive generative models for ODE/SDE propose the addition of noise during the denoising process or "churn" to improve the generation quality [23, 43]. Intuitively, this approach slightly noises the latent at each integration step, and allows the model to correct for previous errors. The impact of this stochastic generation is unclear when it comes to an all-atom latent space. In this context, the additional noise could "pull" the current trajectory out of an unfavorable area of the latent space. We experiment with varying amounts of churn across the integration, where a higher churn value corresponds to more noise re-injected at each step. We find that a lower level of churn  $\leq 0.1$  is more beneficial to generation success in the all-atom latent space. We note that there may be additional tuning done, such as ranges of  $t$  steps to apply churn. The algorithm for stochastic generation is presented in Algorithm 1.

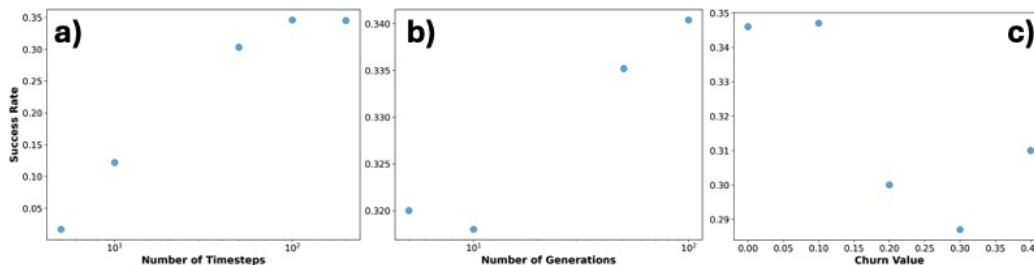


Figure 7: Generation filter success rate for a sample of 100 test polymers vs. A) number of the timesteps, B) number of generations per sample, C) level of churn.

---

**Algorithm 1** PolyGen Generation with Stochasticity

---

**Require:** Polymer connectivity graph  $G$ , number of sampling steps  $T$ , stochasticity level churn

Conditional Encoding  $C_i \leftarrow \mathcal{E}_c(G)$

Set  $\Delta t \leftarrow \frac{1}{T}$

Set  $\gamma \leftarrow \frac{\text{churn}}{T}$

Sample initial latent  $Z_0 \sim \mathcal{N}(0, I)$

Set  $Z_{sc} \leftarrow \emptyset$

**for**  $n \leftarrow 0$  to  $T - 1$  **do**

  Set  $t \leftarrow \frac{n}{T}$

  Sample  $\epsilon \sim \mathcal{N}(0, I)$

$\Delta \hat{t} \leftarrow \gamma(1 - t)$

$\hat{t} \leftarrow \max(t - \Delta \hat{t}, 0)$

$Z_t \leftarrow Z_t + \Delta \hat{t} \sqrt{t^2 - \hat{t}^2} \epsilon$

  Predict  $\hat{Z}_1 = \mathcal{M}(Z_t, Z_{sc}, \hat{t}, C_i)$

$Z_{sc} \leftarrow \hat{Z}_1$

  Compute velocity  $\hat{u}_t = \frac{\hat{Z}_1 - Z_t}{1 - t}$

  Update  $Z_{t+\Delta t} = Z_t + \hat{u}_t \Delta t$

**end for**

Decode final structure:  $\hat{f}, \hat{p}, \hat{b}_z = \mathcal{D}(Z_1, C_i)$

---

## C Model Hyperparameters

Table 1: Hyperparameters for Autoencoder Model

Parameter	Value
<i>General Parameters</i>	
Latent Dimension	8
Learning Rate	$10^{-4}$
Weight Decay	0.0
<i>Architecture</i>	
Token Embedding Dimension	512
Attention Heads	8
Feedforward NN Dimension	1024
Number of Layers	8
<i>Loss Weights</i>	
Loss Weight: Bounding Box (polychain)	1.0
Loss Weight: Bonds (polychain)	2.0
Loss Weight: Angles (polychain)	2.0
Loss Weight: Dihedrals (polychain)	1.0
Loss Weight: Fractional Coordinates (polychain)	10.0
Loss Weight: KL Divergence (polychain)	$10^{-5}$
Loss Weight: Position (qm9)	1.0

Table 2: Hyperparameters for Latent Diffusion Model

<b>Parameter</b>	<b>Value</b>
<i>Architecture</i>	
Latent Dimension	8
Token Embedding Dimension	512
Attention Heads	8
Number of Layers	12
<i>Training</i>	
Learning Rate	$10^{-4}$
Weight Decay	$10^{-4}$
<i>Generation</i>	
Generation Timesteps	100
Churn	0.0